



Effect of volume fraction ratio of Ti to Al₃Ti on mechanical and tribological performances of the in situ Ti–Al₃Ti core–shell structured particle reinforced Al matrix composite

Yuqiang Han¹, Jiayu Liu¹, Qianying Wang¹, Chunfa Lin^{1,a)}, Enhao Wang², Wenwen Wu¹, Mengqiao Zhang¹

¹School of Automotive Engineering, Changshu Institute of Technology, Changshu 215500, China

²School of Materials Science and Engineering, Harbin University of Science and Technology, Harbin 150080, China

a) Address all correspondence to this author. e-mail: chunfalin1852@cslg.edu.cn

Received: 27 July 2022; accepted: 12 September 2022; published online: 21 September 2022

In present work, Ti–Al₃Ti core–shell structured particle reinforced Al matrix composites were fabricated via powder metallurgy technique followed by annealing process. The results indicated that via adjusting annealing parameters, Ti–Al₃Ti core–shell particles with 8:0, 2:1, 1:1, and 1:15 volume fraction ratio of Ti to Al₃Ti, respectively, were in situ formed in the prepared composites. With the reduction of volume fraction ratio of Ti to Al₃Ti, the compressive strength of the composite increases gradually. Besides, as the volume fraction ratio of Ti to Al₃Ti reaches 1:1, the composite shows the best wear resistance among these studied specimens. Furthermore, the relationship between sliding time and wear mechanisms of the composite was investigated in detail via friction and wear tests. As the sliding time increased constantly, the main wear mechanism of the composite is changed from adhesion wear to a combination of fatigue, adhesion, oxidation, and abrasion wear.

Introduction

It is well known that particle reinforced aluminum matrix composites (PRAMCs) possess outstanding performances including superior specific strength, wear resistance, and adjustable elastic modulus [1, 2]. Thus, the PRAMCs are considered as a promising candidate to be applied in aerospace, automobile, and electronics industries [3, 4]. The ceramic (normally SiC [5, 6], TiB₂ [7], and Al₂O₃ [8]) or intermetallic particulates (Al₃Ti [9], Al₃Ni [10]) are always used as reinforcements to synthesize PRAMCs, which can improve the strength of the composite significantly but decrease the ductility and wear resistance. There exist two main reasons for the decline of the ductility and toughness: (1) the interfacial bonding between reinforcement and matrix is weak due to their poor wettability, which leads to crack nucleation and propagation along the interface preferentially during deformation [11, 12], (2) the brittle ceramic or intermetallic particulates will be fractured more easily than the plastic Al matrix when the load is transferred from the matrix to the reinforcements [13], meanwhile, these hard broken particles

are too difficult to depart from the wear surface during friction progress, causing an aggravation of wear [14].

Aim to overcome the problems, one of the most prospective approaches is to prepare the metal–intermetallic core–shell structured particle reinforced aluminum matrix composite via in situ method [15–18]. On the one hand, the reinforcements are formed by in situ chemical reaction between main powder particles during fabrication process, which is beneficial for obtaining strong reinforcement/matrix interfacial bonding to transfer the applied load [19]. On the other hand, the soft aluminum matrix and metal core can provide resistance to the crack propagation as a result of blunting the two tips of the crack, which can delay the fracture of the reinforced particle and further ameliorate mechanical performance and wear resistance of the composite effectively [20]. Recently, Wang et al. [17] and Xue et al. [18] designed and prepared a Fe–Al_xFe_y core–shell structured particle reinforced Al matrix composite by in situ powder metallurgy technique under Ar atmosphere. The results showed that compared to previous Al matrix composites reinforced by ceramic

or intermetallic particulates, the new type of PRAMC possessed a good combination of high strength and compressive ductility. However, some pores were always generated in the composite during sintering ascribed to the Kirkendal effect, which resulted in a substantial drop in tensile ductility. Wu et al. [16] achieved the Ni–Al_xNi_y core–shell structured particle reinforced Al matrix composite via the same method and explored the effect of Ar and N₂ atmosphere on the microstructure and mechanical properties of the composite. It was indicated that under N₂ atmosphere, the reaction of Al with N₂ was occurred, producing the AlN in the pores. Therefore, the porosity of the composite under N₂ atmosphere was less than that under Ar atmosphere, which had advantages on improving the density of the composite. While the ductility was still slightly declined owing to the net-like distribution of AlN. Recently, in situ Ti–Al₃Ti core–shell structured particle reinforced Al matrix composite has been proposed [15, 20, 21]. Their experimental results indicated that the composite exhibited high strength and excellent tensile elongation. The outstanding mechanical performances of the composite were attributed to the Al₃Ti phase, which possessed more favorable properties compared to other Al-rich aluminides [22, 23]. In addition, the volume expansion is relatively low during the generation of Al₃Ti, which is conducive to reducing the porosity of the composite [15]. While at present, the investigations related to the influence of the relative content of Ti core and Al₃Ti shell in the reinforcing particle on the mechanical and tribological performances of the composite have been reported seldom, thus, further researches are urgent to be conducted.

Based on the previous studies, it is necessary to develop the proper quantitative relationship between Ti and Al₃Ti, which will contribute to achieve the excellent comprehensive performance of the composite, and then lay the foundations for its engineering applications. Therefore, the main contents of this work were as follows: firstly, the Ti_p/Al green compact was obtained via powder metallurgy technique. Then, the compact was annealed under Ar atmosphere for different time to achieve Ti–Al₃Ti core–shell structured particle reinforced Al matrix composites with various volume fraction ratios of Ti to Al₃Ti. Thirdly, the microstructure of the composites was characterized by SEM, EDS, and XRD analysis. Finally, nanoindentation, quasi-static compression, and friction–wear tests were carried out on the composites at room temperature to discuss the influence mechanisms of volume fraction ratio of Ti to Al₃Ti on the performances of the composite in detail.

Results and discussion

Phase composition

Figure 1 shows the XRD patterns of the prepared Al matrix composites after annealed at 650 °C for 0.5, 0.75, 1, and 2 h,

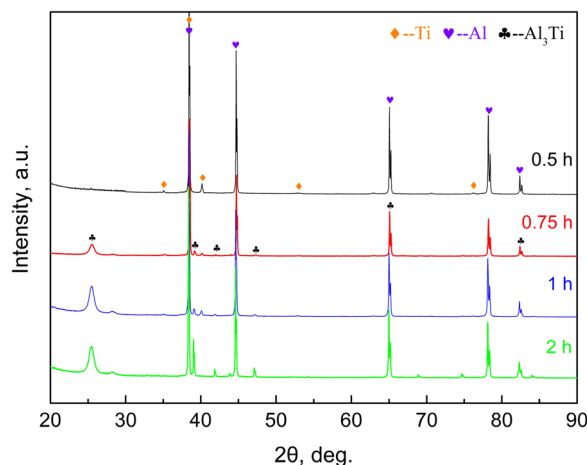


Figure 1: The XRD patterns of the Ti–Al₃Ti core–shell structured particle reinforced Al matrix composites after annealed at 650 °C for 0.5, 0.75, 1, and 2 h, respectively.

respectively. It can be seen that only Ti and Al diffraction peaks with high intensity can be detected in the composite annealed for 0.5 h, revealing there is no new phase formed during this process. While the diffraction peaks corresponding to Al₃Ti phase appear, meanwhile, the intensity of Ti peaks decrease in the composites after annealed for 0.75 and 1 h, which prove that a portion of Ti was converted to Al₃Ti phase by the reaction of Ti + 3Al → Al₃Ti. As the annealing time increases to 2 h, the Ti diffraction peaks disappeared in the XRD pattern of the composite and the Al₃Ti peaks are intensified significantly, indicating that most Ti particles were exhausted and transformed into Al₃Ti.

Microstructure observations

After hot pressing and annealing process, the desired composites with different content of each component were obtained successfully. The back scattered electron SEM images of the synthesized composites are shown in Figs. 2(a)–2(d). As indicated in Fig. 2(a), Ti particles in polygonal shape and light-gray color are evenly dispersed in the Al matrix of the composite annealed for 0.5 h. Under high magnification, the interface between Ti particle and Al matrix is smooth and there is no obvious reaction layer formed at the Ti/Al interface. After annealing for 0.75 h, the reaction of Ti/Al is occurred and a newly formed shell with uniform thickness and consisting of gray phase is observed around the Ti core [see Fig. 2(b)], suggesting the generation of the core–shell structured particles in the composite. Additionally, both of the Ti/shell and shell/Al interfaces are smooth and clean, there no pores exist along the interface. With the annealing time prolong to 1 h, the thickness of shell increases obviously, as can be seen in Fig. 2(c). Besides, it is worth noting that some Ti cores are consumed to convert into the gray phase

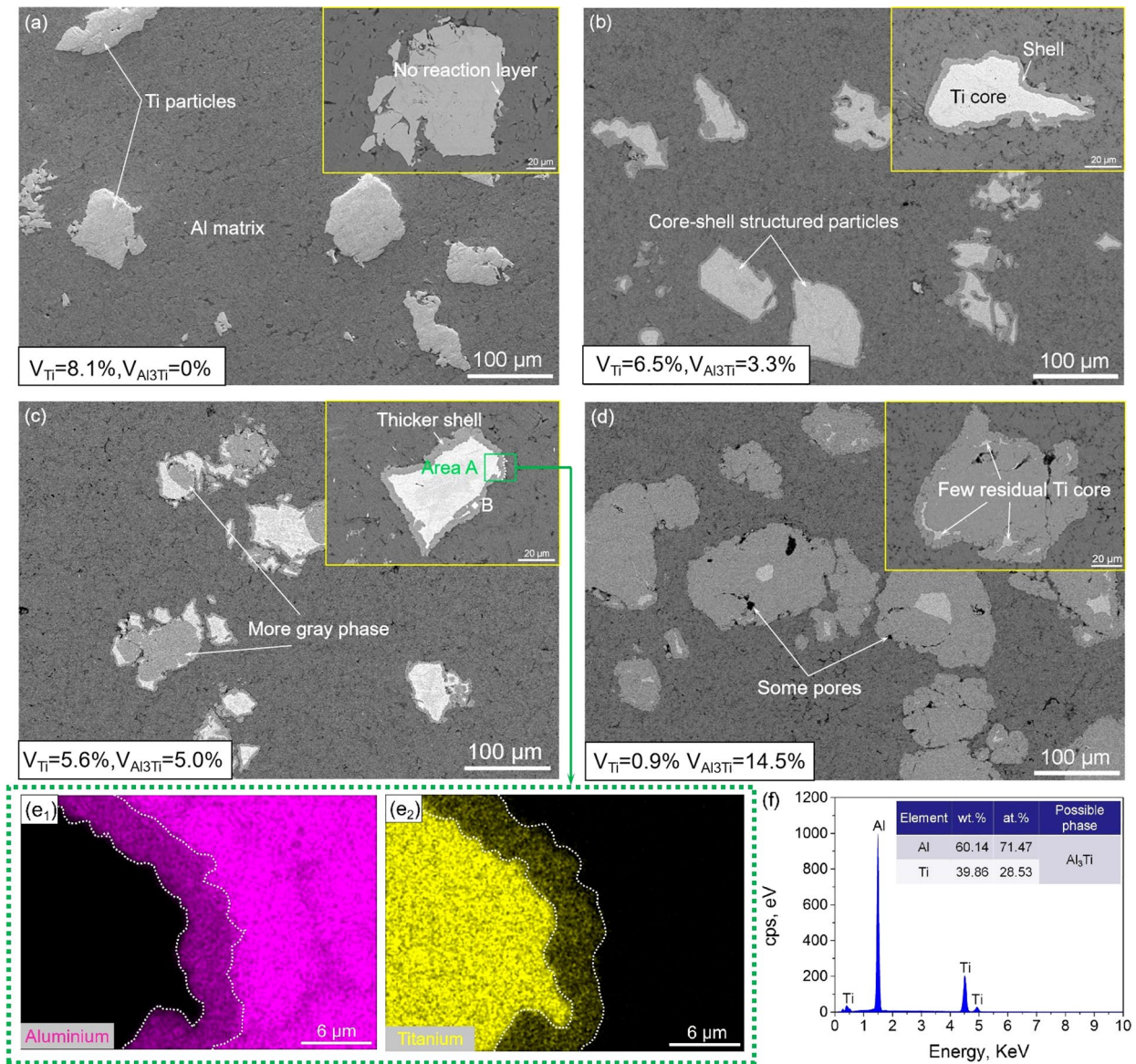


Figure 2: The back scattered electron SEM images of the composites after annealed at 650 °C for 0.5 h (a), 0.75 h (b), 1 h (c), and 2 h (d) and the EDS results (e, f) detected on Area A and Point B as marked in (c).

in the composite annealed for 1 h, implying that Al atoms diffuse across the shell to react with Ti atoms. Some previous investigations [24–26] have also displayed this phenomenon and clarified that Al is the dominant diffusion species at temperature below the melting point of aluminum (660 °C). When the annealing time extends to 2 h, Ti react with Al sufficiently to transform into the gray phase and few residual Ti core can be found in the composite, as show in Fig. 2(d). Furthermore, some pores can be seen in the newly formed gray phase and at the interface of particle/Al matrix, which is attributed to the Kirkendall effect [27–30]. The average size of the reinforced particles in these prepared composites annealed for 0.5, 0.75, 1, and 2 h are statistically analyzed based on SEM images under low magnification,

which corresponding to 79.2, 93.0, 98.6, and 121.4 μm, respectively. It is noted that the size of particle is increased gradually as a result of the occurrence of Ti/Al interfacial reaction. In order to further analyze the element distribution and phase composition of the shell, EDS mapping and point analyses were performed in the Area A and Point B [marked in Fig. 2(c)] in the composite annealed for 1 h and the results were presented in Figs. 2(e) and 2(f), respectively. Obviously, from Figs. 2(e1) and 2(e2), the shell is a Al- and Ti-rich mixed zone, revealing that the Al atom diffused from Al matrix into Ti particle and the Ti atom diffused in the opposite direction during the annealing process. The atom percent ratio of Al to Ti in shell is close to 3:1, as indicated in Fig. 2(f). Combined with the XRD result shown

in Fig. 1, it can be concluded that the in situ generated shell comprises Al_3Ti phase, which is in a good agreement with the results reported by Guo et al. [15, 20] and Junqani et al. [19] and the reasons for the formation of Al_3Ti as only reaction product have been explained in many previous literatures [31–33].

Moreover, the volume fraction of Ti and Al_3Ti phases in the composites after annealed for 0.5, 0.75, 1, and 2 h can be estimated according to the quantitative metallography and stereology theories based on the SEM images of randomly selected area under the same low magnification. The detailed results are marked in Figs. 2(a)–2(d). It can be found that the volume fraction ratios (VFR) of Ti core to Al_3Ti shell in the composites are approximately corresponding to 8:0, 2:1, 1:1, and 1:15, respectively, which decrease with the increase of annealing time. There are two major factors accounting for this phenomenon. One, extending annealing time can accelerate atomic diffusion, another, longer annealing time can reduce the free energy of the formation of Al_3Ti through releasing more heat, both of which promote the consumption of Ti and the nucleation as well as the growth of Al_3Ti . For the convenience of description, the composites are named separately as VFR-8/0, VFR-2/1, VFR-1/1, and VFR-1/15, according to the volume fraction ratio of Ti to Al_3Ti .

Composite properties

Density and nanoindentation

The bulk density and relative density of the prepared Ti– Al_3Ti core–shell structured particle reinforced Al matrix composites are presented in Fig. 3(a). With the increase of annealing time, the relative density of the VFR-8/0, VFR-2/1, and VFR-1/1 composites increases gradually from 92.2 to 96.9%, which is attributed to the atomic diffusion of Ti and Al during the initial period of reaction in favor of reducing the proportion of tiny pores. Besides, the changes in bulk density of these composites are similar with those of relative density, owing to the increasing content of Al_3Ti shell. However, as annealing time is further prolonged to 2 h, both the bulk density and relative density decrease visibly caused by the accumulation of numerous vacancies to generate some new pores during the formation of extensive Al_3Ti phase, which is coincident with the result of SEM observation, as shown in Fig. 2(d). Therefore, when the volume fraction ratio of Ti to Al_3Ti is 1:1, the relative density of the composite reaches the maximum, which plays a role in improving the performances of the Ti– Al_3Ti core–shell structured particle reinforced Al matrix composite.

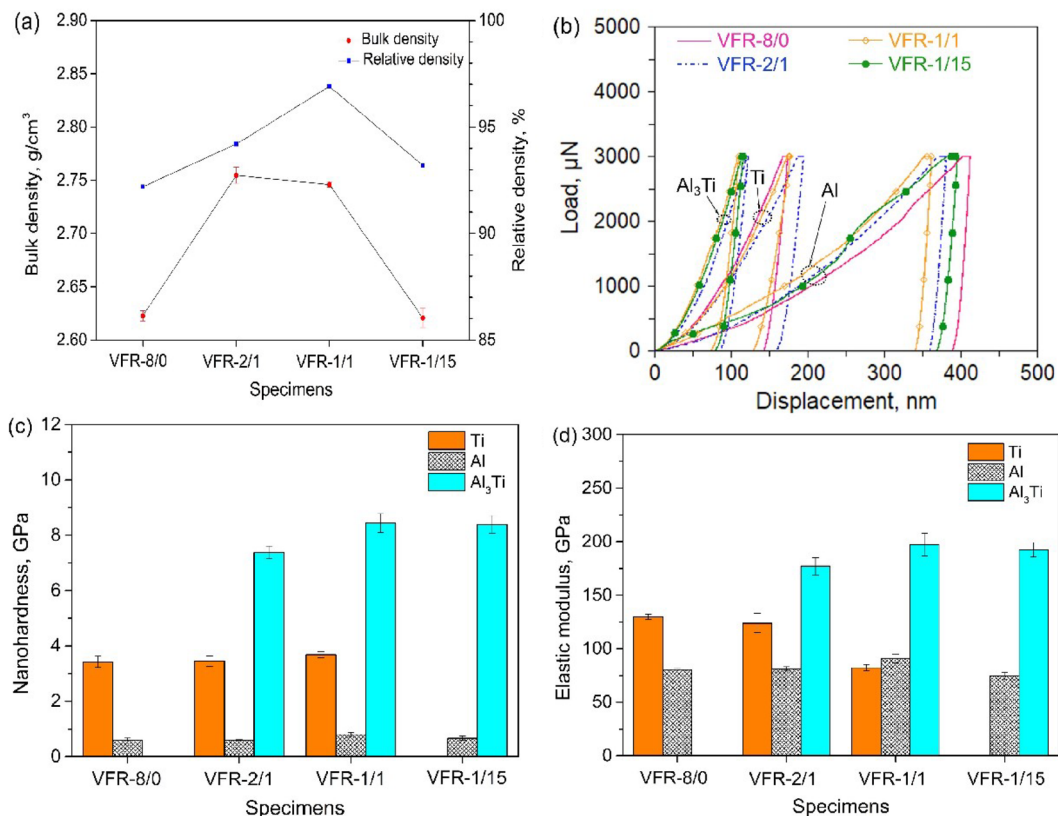


Figure 3: The density and nanoindentation of the Ti– Al_3Ti core–shell structured particle reinforced Al matrix composites.

Figures 3(b)–3(d) display the typical load–displacement curves and the histograms corresponding to nanohardness and elastic modulus of each component in the prepared Al matrix composites after nanoindentation tests. It can be seen in Fig. 3(b) that both the maximum displacement and the shape of curves vary slightly with the annealing time, suggesting that minor fluctuations exist in the nanohardness and elastic modulus of those components. Notably, the average nanohardness (H) of Ti in the VFR-1/1 composite after annealed for 1 h reaches to the highest (3.69 GPa), compared with those in VFR-8/0, VFR-2/1, and VFR-1/15 composites, as shown in Fig. 3(c). On the contrary, the average elastic modulus (E) of Ti reduces apparently to 82.25 GPa in the VFR-1/1 composite [see Fig. 3(d)]. It has been proposed that as the Ti/Al solid-state reaction proceeded, numerous Al atoms diffused from Al matrix to Ti particle and were dissolved in Ti crystal lattice. Then, the lattice distortion was occurred in Ti, resulting in the changes in nanohardness and elastic modulus of Ti [34]. Additionally, with the formation of extensive Al_3Ti phase, the nanohardness and elastic modulus of Al_3Ti are gradually tending toward stability. The results are close to those measured by the same method in Lin et al.'s work [35]. Moreover, some previous works implied that the ratios of H^3/E^2 and H/E are regarded as important indicators related to the property of wear resistance of materials [36–38]. The corresponding mechanical parameters of each component in these composites can be calculated based on the Figs. 3(c) and 3(d), and are listed in Table S1. The H^3/E^2 and H/E values of Ti core, Al_3Ti shell and Al matrix in the VFR-1/1 composite are higher than those in other three composites, indicating that it is beneficial to improve wear resistance of the VFR-1/1 composite.

Compressive behavior

Figures 4(a) and 4(b) show the typical compressive stress–strain curves and the histograms of compressive strength of the Ti– Al_3Ti core-shell structured particle reinforced Al matrix composites, respectively. It can be found in Fig. 4(b) that the average compressive strength values of the VFR-8/0, VFR-2/1, VFR-1/1, and VFR-1/15 composites are 150 MPa, 168 MPa, 176 MPa, and 211 MPa, respectively. Namely, with the decrease of volume fraction ratio of Ti to Al_3Ti in the core-shell structured particles, the compressive strength of the composite increases gradually. Figures 4(c)–4(f) display the SEM images of the deformed surface for the composite specimens after compression. From Fig. 4(c), it is clear that the cracks are formed and propagated in both Al matrix and Ti particle during deformation of the VFR-8/0 composite. In addition, the interface debonding is occurred between Al matrix and Ti particle in this composite owing to their weak physical bonding, which has negative influence on the strength of the composite. While in the VFR-2/1 composite after annealed at 650 °C for 0.75 h, a thin Al_3Ti shell was in situ

formed between Al matrix and Ti core, resulting in the transformation of physical connected interface into chemical bonding interface. According to the calculation of interfacial mismatch strain between Al and Al_3Ti [9, 15, 20], a coherent boundary between Al and Al_3Ti was obtained, and therefore the applied load can be transferred from soft Al to Al_3Ti with strong bearing capacity effectively. It has also been verified by the deformed surface observation, as indicated in Fig. 4(d). Obviously, cracks are nucleated and propagated in Al_3Ti shell leading to the fracture of Al_3Ti , which is beneficial for improving the composite strength.

As annealing for 1 h, higher volume fraction of Al_3Ti shell was produced in VFR-1/1 composite, leading to higher compressive strength of this composite, compared with that of VFR-2/1 composite [see Fig. 4(a)]. Previous investigations also indicated that more amount of Al_3Ti can further raise the strength of in situ $\text{Al}_3\text{Ti}_p/\text{Al}$ composites [39, 40]. It can be found in Fig. 4(e) that the cracks were prior to be formed in Al_3Ti shell, then extended to Ti core and Al matrix, owing to the superior load transfer efficiency between Al matrix and reinforcement particles. While the further propagation of crack can be hindered, suggesting that the delayed fracture of the composite was obtained. As for the VFR-1/15 composite annealed for 2 h, the Al_3Ti shell proportion reaches majority and compressive strength of the composite is the highest among these composites. However, it is inconsistent with the results reported in Guo et al.'s work [20], in which the tensile strength of the composite decreased once most of Ti were converted to Al_3Ti , as a result of the existence of pores at the interface of $\text{Al}_3\text{Ti}/\text{Al}$. In this study, the pores can be closed under the compressive stress. Therefore, no pores can be seen in the VFR-1/15 composite after compression tests, as shown in Fig. 4(f). In addition, it is noted that the main crack is prior to nucleate and branch into secondary cracks in the Al_3Ti . While there exists minor volume fraction of residual Ti core, which has an adverse effect on confining the crack propagation and further accelerates the fracture process of the composite.

Tribological properties

As we all know, the addition of particle reinforcements plays an important role in improving wear resistance of Al matrix composite. Thus, it is necessary to study the influence mechanisms of the volume fraction ratio of Ti to Al_3Ti on the wear resistance of the Ti– Al_3Ti core-shell structured particle reinforced Al matrix composite. Figure 5 shows the profiles of worn track on the VFR-8/0, VFR-2/1, VFR-1/1, and VFR-1/15 composites after friction and wear tests. The cross-sectional areas (S) of worn track are measured by profile instrument and the corresponding wear volumes (ΔV) are calculated by Eq. (4). The details can be seen in “Experimental procedures” section. Based on the Eq. (3), the lower wear rate, the less wear volume under the same

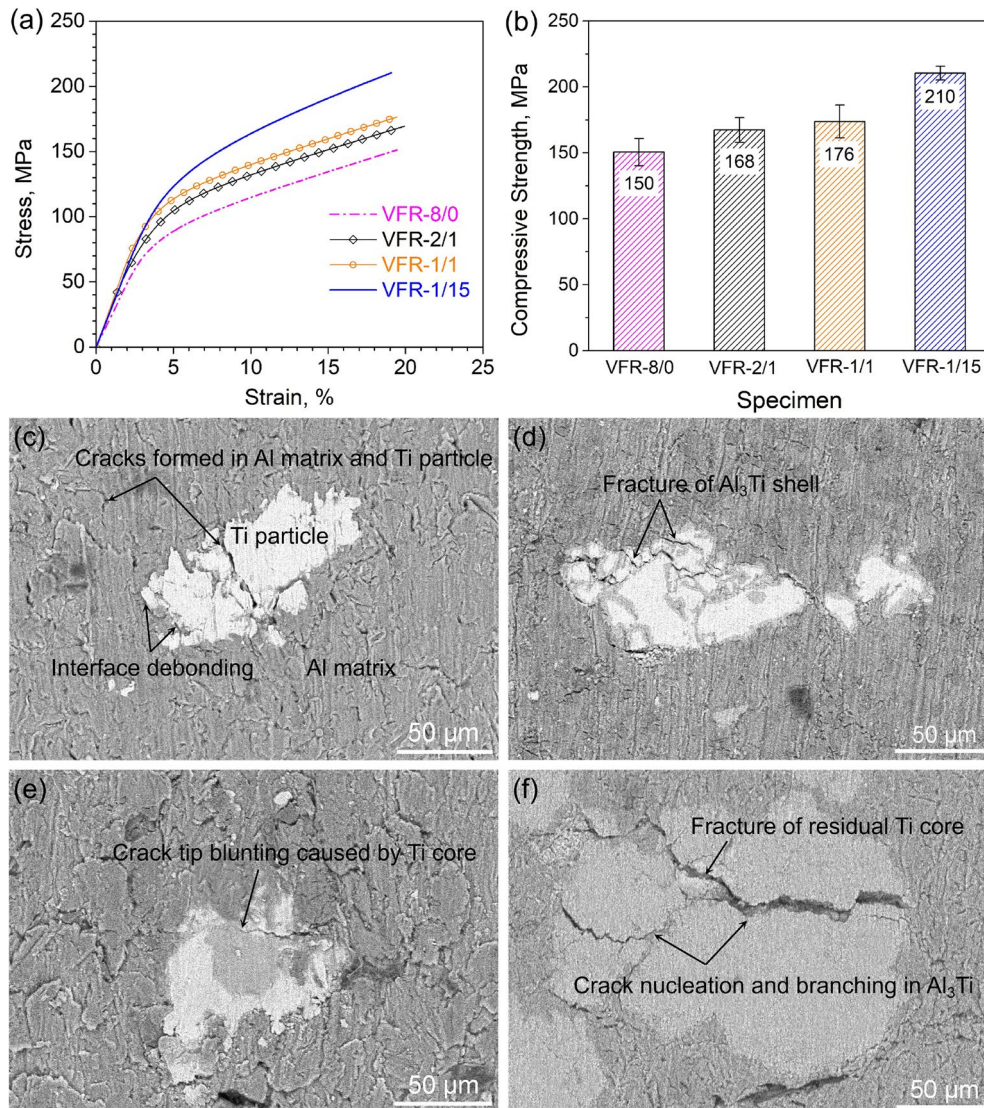


Figure 4: The compressive stress–strain curves (a) and the histogram of compressive strength (b) of the prepared composites as well as the SEM images of deformed surface corresponding to VFR-8/0 (c), VFR-2/1 (d), VFR-1/1 (e), and VFR-1/15 (f) composites, respectively.

condition, implying that the composite possesses superior wear resistance. The calculation results of the wear rate are summarized in Fig. 6(a), the composite can be arranged in an ascending order of wear rate (K): VFR-1/1, VFR-1/15, VFR-2/1, and VFR-8/0 under all tested time, implying that the VFR-1/1 composite exhibits superior wear resistance compared with other three composites. In addition, with increasing sliding time, the K of all composites increases slightly. The trend of wear rate will be explained and discussed by the microstructure observation of worn surface later in this section.

Moreover, the variation of friction coefficient versus sliding time of VFR-8/0, VFR-2/1, VFR-1/1, and VFR-1/15 composites are displayed in Fig. 6(b). It can be seen that the average friction coefficient of the VFR-8/0 composite is 0.183

under the sliding time of 20 min. In comparison, the average friction coefficients decrease gradually to 0.161, 0.105 for VFR-2/1 and VFR-1/1 composites, respectively, then rise to 0.123 for the VFR-1/15 composite. Meanwhile, the friction coefficients of all composites are proportional to the sliding time. As indicated in Fig. 5, it can be found that obvious material pile-ups exist on the edge of all the worn tracks, as marked with white arrows, which is attributed to the materials deformation [41]. Besides, a number of scratches (black arrows) can be observed on the surface of worn track, when the sliding time was 20 min. As prolonging the sliding time, the scratches blurred gradually and distinct plastic deformation (orange arrows) is formed on the worn track, revealing that the surface thermal softening was occurred owing to the friction

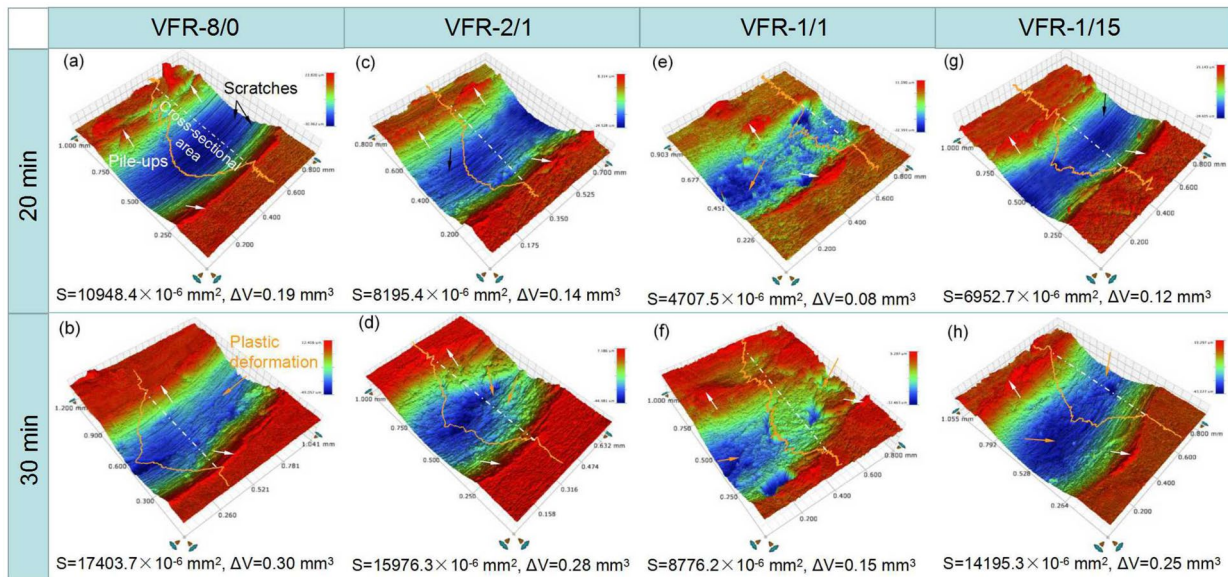


Figure 5: Profiles of worn tracks on the VFR-8/0, VFR-2/1, VFR-1/1, and VFR-1/15 composites after friction and wear tests.

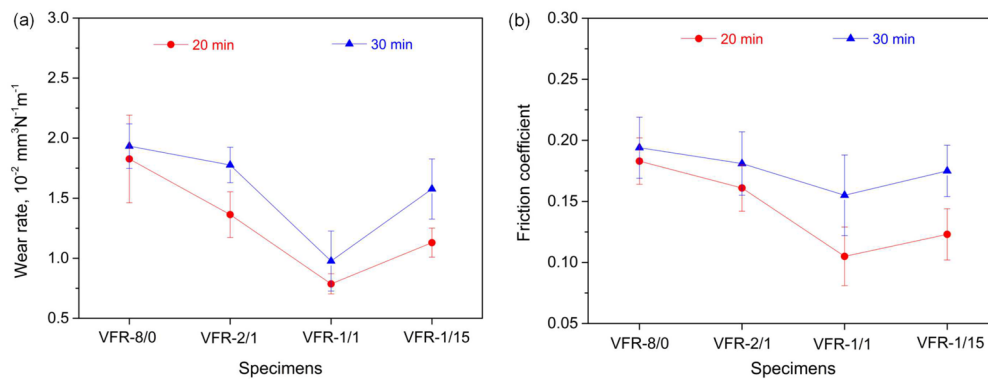
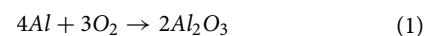


Figure 6: The wear rate (a) and friction coefficient (b) of the Ti-Al₃Ti core-shell structured particle reinforced Al matrix composites tested for 20 and 30 min.

heat. In this case, the effect of adhesion will be enhanced, which has an increasing effect on the friction coefficient of the composite. Furthermore, the results of compression test (in Fig. 4) imply that the fracture of Ti-Al₃Ti core-shell particles in the VFR-1/1 composite can be delayed. Namely, under the external load, the particles are able to support the main load rather than falling out of the matrix rapidly. Since the higher hardness of the Ti-Al₃Ti core-shell particles, the softer Al matrix around the particles is more prone to be worn out during the sliding process. Then, the particles protrude from the surface of the VFR-1/1 composite, reducing the contact area between GCr15 ball and Al matrix, which is responsible for the relatively lower friction coefficient of VFR-1/1 composite, compared to those of VFR-8/0, VFR-2/1, and VFR-1/15 composites.

Wear mechanisms

Figure 7 presents the morphologies of worn track on the composite specimen. The EDS elemental distribution maps (Figs. S1–S8) of the selected region marked by orange dotted line in Fig. 7 indicate that aluminum and oxygen elements are the major components of worn track and some titanium-rich zones can be detected on the worn track. The mass fraction of each element on worn track is listed in Table S2. It can be found that the mass fraction of oxygen element increases with extending of sliding time, suggesting that surface oxidation was aggravated on the worn track as the interface frictional heat raised during friction and wear process in air [41–44]. Here, the Al matrix and Ti core may be oxidized to generate Al₂O₃ and TiO₂, the details are as follows:



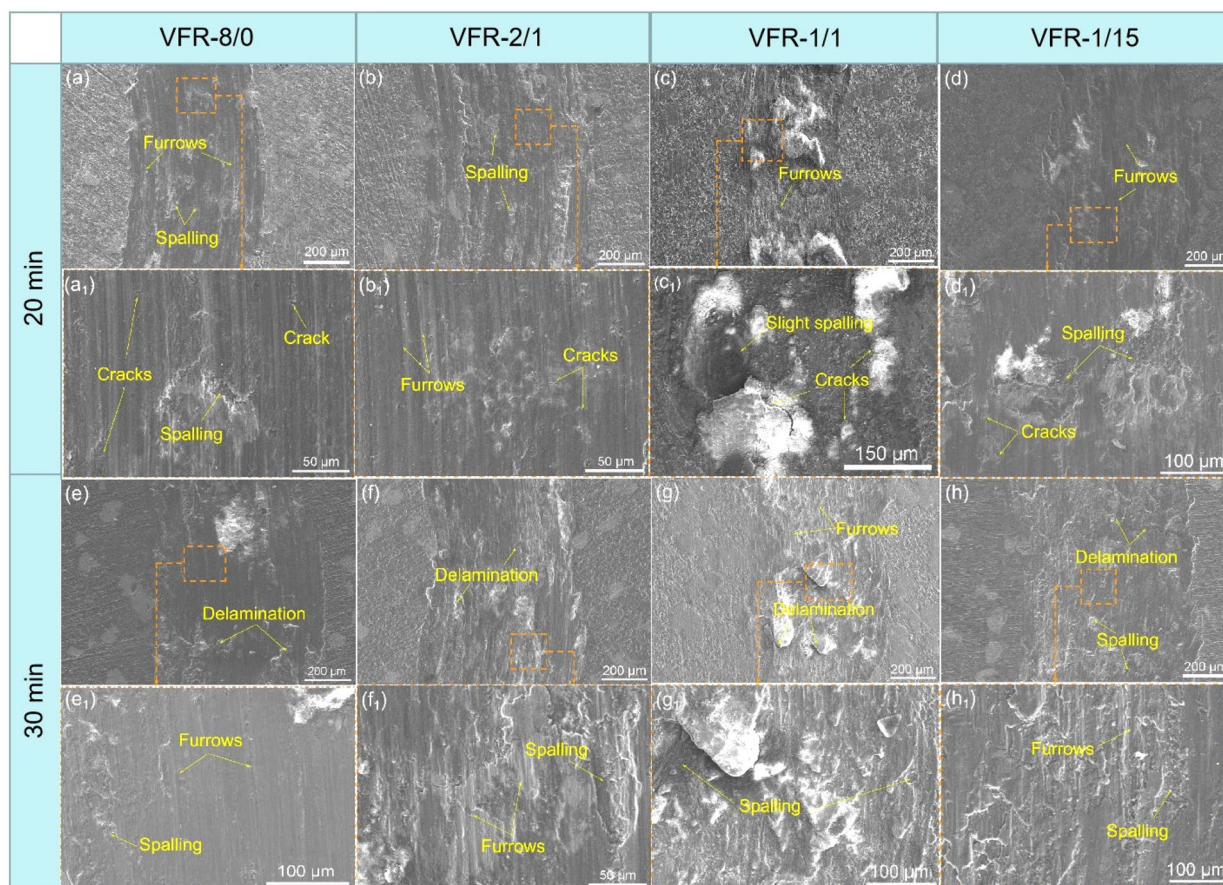


Figure 7: Morphologies of worn track on the VFR-8/0, VFR-2/1, VFR-1/1, and VFR-1/15 specimens after friction and wear testing.



Figures 7(a)–7(d) show the morphologies of worn track on the composite specimens after sliding for 20 min. Obvious spalling and some furrows with shallow and narrow shape can be seen on the worn track of the specimens, revealing that adhesion is the major mechanism of wear and abrasion plays the secondary role [45]. Namely, under the cycle stress exerted by friction pair, adhesion may occur between micro-protrusions on the surface of the specimen and friction pair due to local high pressure, then the adhesive points are teared and pulled during sliding, resulting in a large amount of spalling, which implies the adhesion wear. Besides, the hard phases peel off and shear the surface of the specimens, leading to some furrows on the worn track, which is the typical features of abrasion wear. Furthermore, some cracks can be observed on the worn tracks perpendicular to the sliding direction, revealing the fatigue wear. This is induced by the strain accumulation to a critical level during the repeated sliding friction process [41]. Thus, the wear mechanisms of the composites become a combination of adhesion, abrasion, oxidation, and fatigue wear under the 20 min

sliding time. When the sliding time increase to 30 min, as shown in Figs. 7(e), 7(h), the worn tracks present severer wear with numerous delamination layers and spalling, displaying serious fatigue wear and adhesion wear. Besides, the oxidation is another major factor of the wear, as a result of numerous oxygen element detected on the worn track via EDS mapping analysis. Oppositely, the furrows cannot be observed clearly on the worn track, revealing a slight abrasive wear. Thus, as the sliding time increased continuously, the main mechanism of the composites is converted into severer wear with the comprehensive impact of fatigue, adhesion, oxidation, and abrasion, eventually leading to the increase in wear rate. Moreover, it is worth noting that the worn track on VFR-1/1 specimen is obviously distinguished from those on VFR-8/0, VFR-2/1, and VFR-1/15 specimens, as shown in Figs. 7(c) and 7(g). Based on the EDS mapping results (Figs. S1–S8), it can be found that shear was commonly occurred at Al_3Ti shell. However, it is notable that the particles are not nearly detached from the matrix during the sliding process, which is attributed to the inhibition of Ti core and Al matrix on the crack propagation and the delayed fracture of reinforced particles. In this case, the load carrying effect of the Ti- Al_3Ti core-shell particles can be utilized completely, which

is beneficial for improving the wear resistance of the composite. Additionally, high relative density plays a positive role in improving wear resistance of the composite under dry conditions. According to the former analysis, it can be found that the relative density of the VFR-1/1 composite is higher than those of VFR-8/0, VFR-2/1, and VFR-1/15 composites [see Fig. 3(a)], suggesting that less micro-defects exist in the VFR-1/1 composite, which can alleviate the abrasion wear [46]. Furthermore, the ratios of H^3/E^2 and H/E represent plastic deformation resistance and maximum bearing capacity of the material maintaining the elastic limit during the friction process, respectively [36]. As mentioned above, the components in VFR-1/1 composite possess higher H^3/E^2 and H/E values, compared to those in other three composites, which contributes to superior wear resistance of the VFR-1/1 composite.

In summary, through the contrastive analysis, the VFR-1/1 composite possesses the best wear resistance, the main reasons are as follows: firstly, when the volume fraction ratio of Ti to Al_3Ti is 1:1, the cracks propagation can be inhibited by Ti core and Al matrix effectively, which is favorable for delaying the fracture of reinforced particles during friction and wear test. The reinforced particles with strong bearing capacity are responsible for superior wear resistance of the composite. Secondly, higher relative density is conducive to reduce stress concentration in the composite, which also has advantages on raising wear resistance of the composite. Finally, Ti core, Al_3Ti shell, and Al matrix in VFR-1/1 composite show relatively higher H^3/E^2 and H/E values, which can improve wear resistance of the composite effectively.

Figure 8 shows the wear schematic diagrams of the Ti- Al_3Ti core-shell structured particle reinforced Al matrix composite specimens against the GCr15 ball. Under the load applied by

friction pair, plastic deformation is produced on the surface of specimens and then the material pile-ups are appeared on either side of the worn track, which can be also observed in the profiles of worn tracks, as shown in Fig. 5. Owing to the frictional heat, some oxides, such as Al_2O_3 and TiO_2 , are formed on the worn track. While these oxides are brittle and easily fell off to be wear debris during the sliding friction test, causing the acceleration of wear process. In addition, the softer Al matrix is prior to be worn away under the action of friction pair, resulting in the reinforced particles with higher hardness protruding from the surface gradually. Then, one possible fact is that many particles are detached from the Al matrix, which plays an important role in enhancing the average friction coefficient and average wear rate of the composites, such as VFR-8/0, VFR-2/1, and VFR-1/15. Another possibility is that the protruding particles act as the major supporting body of the load exerted by friction pair, instead of being peeled off completely. As a result, obvious reductions of both friction coefficient and wear rate are presented in the VFR-1/1 composite. As the sliding time increased to 30 min, the thermal softening of Al matrix is occurred due to the frictional heat. This would increase direct contact area between specimen surface and GCr15 ball as well as prevent the wear debris from being discharged immediately, inducing the aggravation of adhesion wear and fatigue wear, which increases the friction coefficient and wear rate. From Fig. 6, it is also demonstrated that the friction coefficients and wear rates of composites have been on the rise with the extension of sliding time.

Therefore, on the basis of the microstructure observation and performance evaluation of the VFR-8/0, VFR-2/1, VFR-1/1, and VFR-1/15 composites, it can be concluded that the performances of the Ti- Al_3Ti core-shell particle reinforced Al matrix composite can be designed by adjusting the volume fraction ratio of Ti

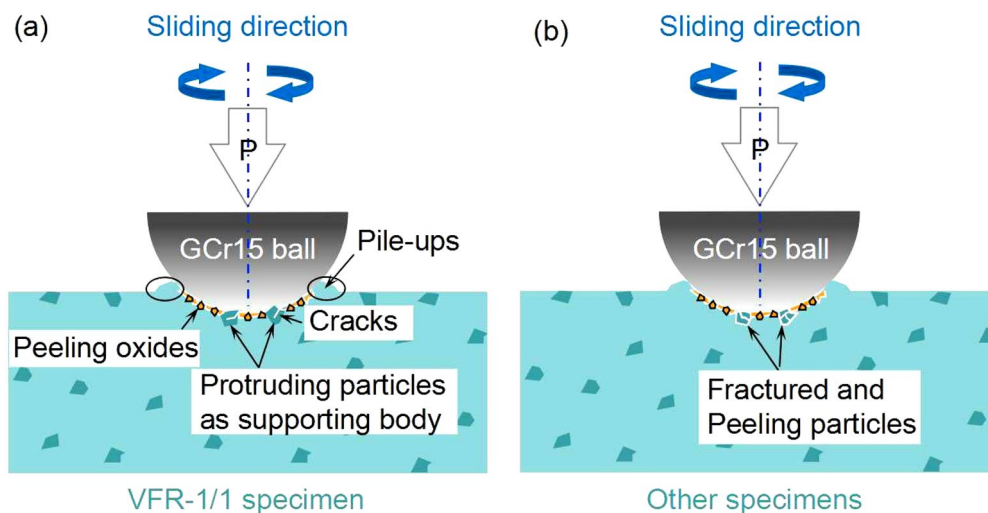


Figure 8: The wear schematic diagrams of the Ti- Al_3Ti core-shell structured particle reinforced Al matrix composite specimens against the GCr15 ball.

to Al_3Ti in the particle through controlling preparation process parameters. When the volume fraction ratio of Ti to Al_3Ti is 1:1, the desired particle/matrix interfacial bonding and proper content of Ti core can be obtained in the composite, which has positive effects on transferring load and preventing the propagation of cracks. As a result, strength and wear resistance of the composite are more excellent than those of the composites with 8:0, 2:1, and 1:15 volume fraction of Ti to Al_3Ti in present work.

Conclusion

In present study, the Ti–Al green compact was obtained through powder metallurgy method, and then it was annealed at 650 °C for 0.5, 0.75, 1, and 2 h, respectively, to synthesize the Ti– Al_3Ti core–shell structured particle reinforced Al matrix composites with various volume fraction ratios of Ti to Al_3Ti . After preparation, the volume fraction ratios of Ti core to Al_3Ti shell in these composites were 8:0, 2:1, 1:1, and 1:15, respectively, which were named as VFR-8/0, VFR-2/1, VFR-1/1, and VFR-1/15 in sequence. The microstructure, mechanical, and tribological properties of the composites were analyzed comparatively to explore the influence mechanisms of volume fraction ratio of Ti to Al_3Ti on the performances of the composite. The main conclusions are as follows:

The relative density of VFR-1/1 composite is 96.6%, which is higher than those of VFR-8/0, VFR-2/1, and VFR-1/15 composites. In addition, Ti core, Al_3Ti shell, and Al matrix in VFR-1/1 composite possess higher H^3/E^2 and H/E values than those in other three composites.

The compressive strength values of the VFR-8/0, VFR-2/1, VFR-1/1, and VFR-1/15 composites are 150, 168, 176, and 210 MPa, respectively, which increase gradually with the reduction of volume fraction ratio of Ti to Al_3Ti .

When the volume fraction ratio of Ti to Al_3Ti is 1:1, the composite possesses the best wear resistance. After sliding for 20 min, the major wear mechanism of the Ti– Al_3Ti core–shell structured particle reinforced Al matrix composite is adhesion wear. As the sliding time increase to 30 min, the primary wear mechanism of the composite transits from adhesion to severer wear with the comprehensive impact of fatigue, adhesion, oxidation, and abrasion.

Experimental procedures

Composite preparation

The starting materials used to fabricate Ti– Al_3Ti core–shell structured particle reinforced Al matrix composite were commercially pure Ti powder (~99.8 wt% purity) and Al powder (~99.9 wt% purity) with the similar particle size of 80~100 μm . The Ti particles are irregular in shape with distinct sharp

corners, while the surface of Al particles is relatively smooth. The Ti and Al powders with weight ratio of 1:9 were ball-milled for 20 min in a planetary powder mixer (Nanjing University Instruments Co., Ltd) in vacuum (10^{-3} Pa) with a rotation speed of 200 rpm. The weight ratio of ball to powder was 10:1. After ball-milling, the shape of powder particles, especially for Ti particle, approaches to ellipsoid and the particle size of powders decreases to 30~70 μm , owing to the occurrence of cold-welding, fracture and recombination of the particles during the process. Besides, the mechanical energy produced by ball-milling can promote atom diffusion at the interface between powder particles [47]. Then, the mixed powders were hot pressed at 600 °C for 1 h in vacuum (10^{-3} Pa) in a cylindrical steel die with the diameter and height of 50 mm and 20 mm, respectively. During the process, the pressure of 200 MPa was remained to accelerate densification of the green compacts. Subsequently, the green compacts were further annealed at 650 °C for 0.5, 0.75, 1, and 2 h, respectively, under Ar atmosphere and then cooled in the furnace in order to achieve the Ti– Al_3Ti core–shell structured particle reinforced Al matrix composites with various volume fraction ratios of Ti to Al_3Ti . The illustrative diagram of the specific preparation process for the desired composites is shown in Fig. 9.

Microstructure characterization

A Hitachi Regulus 8100 scanning electron microscope (SEM) equipped with a XFlash 6|100 energy dispersive spectrometer (EDS) was utilized to investigate the microstructure and chemical composition of the Ti– Al_3Ti core–shell structured particle reinforced Al matrix composites. The phase compositions of the composites were examined by a Rigaku SmartLabSe X-ray diffraction with $\text{Cu K}\alpha$ radiation at the scanning speed of 5°/min. Furthermore, SEM images of different regions on the cross section for each composite specimens were collected under the same low magnification. Then, the volume fraction of the phases

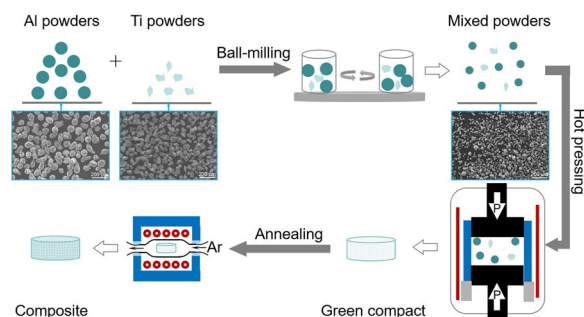


Figure 9: Schematic illustration of preparation process for the desired Ti– Al_3Ti core–shell structured particle reinforced Al matrix composite.

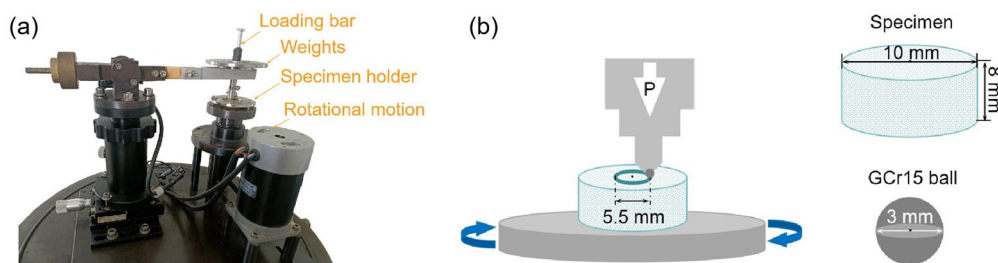


Figure 10: The digital photograph of the tribometer (a) and schematic diagram of friction pair (b).

existing in the composites was statistically calculated according to the quantitative metallography and stereology theories.

Composite properties

The bulk density of the Ti–Al₃Ti core–shell structured particle reinforced Al matrix composites was measured by Archimedes method. The theoretical density can be calculated with the frequently used density of Al₃Ti, Ti, and Al corresponding to 3.36, 4.51, and 2.70 g/cm³. And then the relative density of the composites is equal to bulk density divided by theoretical density. In addition, the hardness and elastic modulus in nanoscale of main components of the composites, including Ti, Al₃Ti, and Al, were estimated on the cross section of the composite specimens via nanoindentation tests using Bruker Hysitron TI980 instrument equipped with the standard berkovich indenter. A load of 3000 μN was applied on the specimens with the loading, holding, and unloading time of 5, 2, and 5 s, respectively. This test was conducted for 3 times on the each selected area to offer the average value of the performance index of Ti, Al₃Ti, and Al phases in the composites.

Besides, the quasi-static compressive tests were performed on the Ti–Al₃Ti core–shell structured particle reinforced Al matrix composite via Instron 5500R load frame at a cross head speed of 2 mm/min and the compressive strength was determined as the compression ratio of 20% at room temperature. The cubic specimens with the dimension of 5 mm × 5 mm × 10 mm machined from the prepared composites were tested under the loading perpendicular to the square end face. It should be pointed out that before compression, the surface of the specimens were polished using the sandpapers in order to reduce the friction between specimen and pressure plate. After compression, the morphology of the area with maximum deformation on the surface of specimens was observed by SEM to investigate the deformation mechanisms of the composites.

Moreover, to establish the relationship between the volume fraction ratio of Ti to Al₃Ti and the wear resistance of the composite, dry sliding friction, and wear experiments at room temperature were carried out on the cylinder specimens

(10 mm in diameter, 8 mm in height), which were cut from the composite and polished to 1000 grit by sandpaper, using a WTM-2E high-speed rotation ball-disc tribometer, as shown in Fig. 10(a). A GCr15 ball (used as metal bearing material in practical production) as a friction pair (diameter: 3 mm) was used to test for 20 and 30 min, respectively, under the load of 1 N and speed of 300 r/min. The friction pair was displayed schematically in Fig. 10(b). Those selected test parameters are in order to avoid the occurrence of melting wear resulted from high load and speed [48]. Notably, the GCr15 ball surface was also treated by the sandpaper, aim to ensure the surface roughness of the GCr15 ball matches with that of the specimen. The friction and wear tests were repeated three times under each experimental conditions. The friction coefficient was obtained directly from a data acquisition system installed inside the computer connected with the experimental device. After the friction and wear tests, the profiles, morphologies, and chemical compositions of the worn tracks were determined by surface profiler (BRUKER GT-K), SEM, and EDS, respectively. The wear rate was calculated by the following Eq. (3) [49]:

$$K = \frac{\Delta V}{L \times d} \quad (3)$$

where K is the wear rate, mm³/N m, ΔV is the wear volume, mm³, L is the load, N and d is the total sliding distance, m.

In this case, the wear volume ΔV in Eq. (3) was

$$\Delta V = S \times C \quad (4)$$

where S is the cross-sectional area of the worn track, mm², which was obtained based on the profiles of the worn track, and C is the circumference of worn track, mm.

Acknowledgments

The authors gratefully acknowledge the financial supports of this study by the Natural Science foundation of Jiangsu Province (Grant No. BK20220690), Initial Scientific Research Fund in Changshu Institute of Technology (Grant Nos. KYZ2018044Q, KYZ2018043Q) and the National Natural Science Foundation of China (No. 51901058).

Data availability

The raw/processed data required to reproduce these findings cannot be shared at this time due to legal or ethical reasons.

Declarations

Conflict of interest The authors declare that they have no known competing financial interests or personal relationships that could have appeared to influence the work reported in this paper.

Supplementary Information

The online version contains supplementary material available at <https://doi.org/10.1557/s43578-022-00742-8>.

References

1. K. Ma, E.J. Lavernia, J.M. Schoenung, Particulate reinforced aluminum alloy matrix composites-A review on the effect of microconstituents. *Rev. Adv. Mater. Sci.* **48**(2), 91–104 (2017)
2. J.M. Torralba, C. Costa, F. Velasco, P/M aluminum matrix composites: an overview. *J. Mater. Process. Technol.* **133**(1–2), 203–206 (2003)
3. S.T. Mavhungu, E.T. Akinlabi, M.A. Onitiri et al., Aluminum matrix composites for industrial use: advances and Trends. *Proc. Manuf.* **7**, 178–182 (2016)
4. R. Casati, M. Vedani, Metal matrix composites reinforced by nano-particles-a review. *Metals-Open Access Metall. J.* **4**(1), 65–83 (2014)
5. X. Deng, N. Chawla, Modeling the effect of particle clustering on the mechanical behavior of SiC particle reinforced Al matrix composites. *J. Mater. Sci.* **41**(17), 5731–5734 (2006)
6. C. Sun, R. Shen, M. Song et al., Mechanical behaviors of SiC particle reinforced Al matrix composites: a study based on finite element method. *Adv. Mater. Res.* **535–537**, 3–7 (2012)
7. Y. Xiong, W. Wang, R. Jiang et al., Tool wear mechanisms for milling in situ TiB₂ particle-reinforced Al matrix composites. *Int. J. Adv. Manuf. Technol.* **86**, 9–12 (2016)
8. Z. Ge, Z. Shi, T. Na et al., Effect of the heating rate on the microstructure of in situ Al₂O₃ particle-reinforced Al matrix composites prepared via displacement reactions in an Al/CuO system. *Mater. Des.* **66**, 492–497 (2015)
9. X. Wang, A. Jha, R. Brydson, In situ fabrication of Al₃Ti particle reinforced aluminium alloy metal-matrix composites. *Mater. Sci. Eng. A* **364**(1–2), 339–345 (2004)
10. F.M. Heim, Y. Zhang, X. Li, Uniting strength and toughness of Al matrix composites with coordinated Al₃Ni and Al₃Ti reinforcements. *Adv. Eng. Mater.* **20**(1), 1700605 (2018)
11. X. Guo, Q. Guo, Z. Li et al., Interfacial strength and deformation mechanism of SiC-Al composite micro-pillars. *Scripta Mater.* **114**, 56–59 (2016)
12. P. Liu, A. Wang, J. Xie et al., Characterization and evaluation of interface in SiC_p/2024 Al composite. *Trans. Nonferrous Metals Soc. China* **25**(5), 1410–1418 (2015)
13. S. Selvakumar, I. Dinaharan, R. Palanivel et al., Characterization of molybdenum particles reinforced Al6082 aluminum matrix composites with improved ductility produced using friction stir processing. *Mater. Charact.* **125**, 13–22 (2017)
14. P. Krishnan, P. Lakshmanan, S. Palani et al., Analyzing the hardness and wear properties of SiC and hBN reinforced aluminum hybrid nanocomposites. *Mater. Today* **62**(2), 566–571 (2022)
15. B. Guo, N. Song, R. Shen et al., Fabrication of Ti-Al₃Ti core-shell structured particle reinforced Al based composite with promising mechanical properties. *Mater. Sci. Eng. A* **639**, 269–273 (2015)
16. W. Wu, B. Guo, Y. Xue et al., Ni-Al_xNi_y core-shell structured particle reinforced Al-based composites fabricated by in-situ powder metallurgy technique. *Mater. Chem. Phys.* **160**, 352–358 (2015)
17. Y. Wang, M. Song, S. Ni et al., In situ formed core-shell structured particle reinforced aluminum matrix composites. *Mater. Des.* **56**, 405–408 (2014)
18. Y. Xue, R. Shen, S. Ni et al., Fabrication, microstructure and mechanical properties of Al-Fe intermetallic particle reinforced Al-based composites. *J. Alloy. Compd.* **618**, 537–544 (2015)
19. M.T. Junqani, H. Hosseini, A. Azarniya, Comprehensive structural and mechanical characterization of in-situ Al-Al₃Ti nanocomposite modified by heat treatment. *Mater. Sci. Eng. A* **785**, 139351 (2020)
20. B. Guo, M. Song, X. Zhang et al., Achieving high combination of strength and ductility of Al matrix composite via in-situ formed Ti-Al₃Ti core-shell particle. *Mater. Charact.* **170**, 110666 (2020)
21. S. Ma, X. Zhang, T. Chen et al., Microstructure-based numerical simulation of the mechanical properties and fracture of a Ti-Al₃Ti core-shell structured particulate reinforced A356 composite. *Mater. Des.* **191**, 108685 (2020)
22. L. Peng, H. Li, J. Wang, Processing and mechanical behavior of laminated titanium-titanium tri-aluminide (Ti-Al₃Ti) composites. *Mater. Sci. Eng. A* **406**(1–2), 309–318 (2005)
23. Y. Huashun, H. Chen, L. Sun et al., Preparation of Al-Al₃Ti in situ composites by direct reaction method. *Rare Met.* **25**(1), 32–36 (2006)
24. X. Cui, G. Fan, G. Lin et al., Growth kinetics of TiAl₃ layer in multi-laminated Ti-(TiB₂/Al) composite sheets during annealing treatment. *Mater. Sci. Eng. A* **539**, 337–343 (2012)
25. Y. Zhao, J. Li, R. Qiu et al., Growth characterization of intermetallic compound at the Ti/Al solid state interface. *Materials* **12**(3), 472 (2019)

26. L. Xu, Y. Cui, Y. Hao et al., Growth behavior of intermetallic compound layer in multi-laminated Ti-Al diffusion couples. *Mater. Sci. Eng. A* **435–436**, 638–647 (2006)
27. M. Yuan, L. Li, Z. Wang, Study of the microstructure modulation and phase formation of Ti Al₃Ti laminated composites. *Vacuum* **157**, 481–486 (2018)
28. M. Tavooosi, The Kirkendall void formation in Al/Ti interface during solid-state reactive diffusion between Al and Ti. *Surf. Interfaces* **9**, 196–200 (2017)
29. N. Thiyaneshwaran, K. Sivaprasad, B. Ravisankar, Nucleation and growth of TiAl₃ intermetallic phase in diffusion bonded Ti/Al metal intermetallic laminate. *Sci. Rep.* **8**, 16797 (2018)
30. Y. He, Y. Jiang, N. Xu et al., Fabrication of Ti-Al micro/nanometer-sized porous alloys through the Kirkendall effect. *Adv. Mater.* **19**(16), 2102–2106 (2007)
31. L. Peng, J. Wang, H. Li et al., Synthesis and microstructural characterization of Ti-Al₃Ti metal-intermetallic laminate (MIL) composites. *Scripta Mater.* **52**(3), 243–248 (2005)
32. C. Lin, F. Jiang, Y. Han et al., Microstructure evolution and fracture behavior of innovative Ti-(SiC_f/Al₃Ti) laminated composites. *J. Alloy Compd.* **743**, 52–62 (2018)
33. Y. Han, C. Lin, X. Han et al., Fabrication, interfacial characterization and mechanical properties of continuous Al₂O₃ ceramic fiber reinforced Ti/Al₃Ti metal-intermetallic laminated (CCFR-MIL) composite. *Mater. Sci. Eng. A* **688**, 338–345 (2017)
34. M. Mirjalili, M. Soltanieh, K. Matsuura et al., On the kinetics of TiAl₃ intermetallic layer formation in the titanium and aluminum diffusion couple. *Intermetallics* **32**, 297–302 (2013)
35. C. Lin, Y. Han, C. Guo et al., Synthesis and mechanical properties of novel Ti-(SiC_f/Al₃Ti) ceramic-fiber-reinforced metal-intermetallic-laminated (CFR-MIL) composites. *J. Alloy Compd.* **722**, 427–437 (2017)
36. S. Lu, L. Wang, J. Zhang et al., Microstructure and tribological properties of laser-cladded Co-Ti₃SiC₂ coating with Ni-based interlayer on copper alloy. *Tribol. Int.* **171**, 107549 (2022)
37. X. Liu, J. Yang, J. Hao et al., A near-frictionless and extremely elastic hydrogenated amorphous carbon film with self-assembled dual nanostructure. *Adv. Mater.* **24**(34), 4614–4617 (2012)
38. T. Weikert, S. Wartzack, M.V. Baloglu et al., Evaluation of the surface fatigue behavior of amorphous carbon coatings through cyclic. *Surf. Coat. Technol.* **407**, 126769 (2021)
39. C.J. Hsu, C. Chang, P. Kao et al., Al-Al₃Ti nanocomposites produced in situ by friction stir processing. *Acta Mater.* **54**(19), 5241–5249 (2006)
40. Q. Zhang, B. Xiao, D. Wang et al., Formation mechanism of in situ Al₃Ti in Al matrix during hot pressing and subsequent friction stir processing. *Mater. Chem. Phys.* **130**(3), 1109–1117 (2011)
41. Y. Wang, C. Wu, L. Zhang et al., Thermal oxidation and its effect on the wear of Mg alloy AZ31B. *Wear* **476**, 203673 (2021)
42. C. Liu, F. Su, J. Liang, Nanocrystalline Co-Ni alloy coating produced with supercritical carbon dioxide assisted electrodeposition with excellent wear and corrosion resistance. *Surf. Coat. Technol.* **292**, 37–43 (2016)
43. J.K. Lancaster, The influence of temperature on metallic wear. *Proc. Phys. Soc.* **70**(1), 112–118 (1957)
44. J. Zhou, D. Kong, Friction-wear performances and oxidation behaviors of Ti₃AlC₂ reinforced Co-based alloy coatings by laser cladding. *Surf. Coat. Technol.* **408**(25), 126816 (2021)
45. K. Zhang, J. Deng, R. Meng et al., Influence of laser substrate pretreatment on anti-adhesive wear properties of WC/Co-based TiAlN coatings against AISI 316 stainless steel. *Int. J. Refract Metal Hard Mater.* **57**, 101–114 (2016)
46. S.C. Lim, J.H. Brunton, The unlubricated wear of sintered iron. *Wear* **113**(3), 371–382 (1986)
47. I.A. Ditenberg, D.A. Osipov, M.A. Korchagin, et al. Influence of ball milling duration on the morphology, features of the structural-phase state and microhardness of 3Ni-Al powder mixture. *Advanced Powder Technology* (2021)
48. J. An, R.G. Li, Y. Lu et al., Dry sliding wear behavior of magnesium alloys. *Wear* **265**, 97–104 (2008)
49. J. Su, J. Teng, Z. Xu et al., Corrosion-wear behavior of a biocompatible magnesium matrix composite in simulated body fluid. *Friction* **10**(1), 31–43 (2022)

Springer Nature or its licensor holds exclusive rights to this article under a publishing agreement with the author(s) or other rightsholder(s); author self-archiving of the accepted manuscript version of this article is solely governed by the terms of such publishing agreement and applicable law.